



Mechanical Properties and Microstructure Transformation Behavior for Welded Joints in Ship Plate Steel with High-Heat Input Welding

Pengyan Zhang, Jian Zhang, and Binzhou Li

Submitted: 17 June 2021 / Revised: 2 August 2021 / Accepted: 6 August 2021 / Published online: 8 September 2021

Mechanical properties and microstructure transformation for welded joints in EH40 ship plate steel were investigated after an electro-gas vertical welding and welding thermal simulation. Effect of the inclusions on the prior to austenite grain size and nucleation of intragranular ferrites (IGFs) was examined. Results indicated that the experimental steel has a good ability for high-heat input welding. Excellent impact toughness at testing temperature of $-20\text{ }^{\circ}\text{C}$ was obtained. An increase in impact energies at $-20\text{ }^{\circ}\text{C}$ for the position away from fusion line (FL) is observed. The average impact energy (177 J) for heat-affected zone by simulation with heat input of 120 kJ/cm is similar with that (165 J) for FL+1 mm by electro-gas vertical welding with heat input of 207 kJ/cm. The TiN particle lost the pinning effect when the peak temperature reached $1400\text{ }^{\circ}\text{C}$. However, the titanium oxide particles play an important role in inhibiting the austenite grain growth because of the high melting point. Three IAFs nucleated on the $\text{TiO}_x\text{-Al}_2\text{O}_3\text{-MgO-MnS}$ particle with the size of $7.6\text{ }\mu\text{m}$ were observed. The inclusion size is not the dominant requirement for the nucleation of IGFs and IAFs. The MnAl_2O_4 and TiO particle have good lattice matching with ferrite, they have a strong ability to promote the nucleation of IAF.

Keywords electro-gas vertical welding (EGW), grain boundary ferrite (GBF), high-heat input welding, inclusion, intragranular acicular ferrite (IAF)

1. Introduction

EH40 ship plate steel is widely used in ship manufacturing due to its good mechanical properties and weldability. In order to increase manufacturing efficiency and decrease costs, a high-heat input welding technology is gradually used for EH40 ship plate steel. The balance between strength and toughness in EH40 ship plate steel will be ruined if the steels are subjected to the welding thermal cycle characterized by low cooling rate and high peak temperature, producing poor impact toughness for welded joints, especially coarsen grained heat affected zone (CGHAZ) close to the fusion line characterized by the peak temperature up to $1400\text{ }^{\circ}\text{C}$ or higher (Ref 1). A high-heat input welding can lead to significant austenite coarsening and some brittle microstructure, such as grain boundary ferrite (GBF), upper bainite (UB), and ferrite side plate (FSP), resulting in toughness reduction.

It is widely believed that the fine austenite grain and the intragranular acicular ferrite (IAF) provide the optimum microstructure for weld metal and CGHAZ. It is believed that oxides, carbides or nitrides can effectively refine the austenite grain at high temperatures by pinning effect (Ref 2-5). Sha et al.

(Ref 6) demonstrated that Ti-rich carbonitrides inhibited the growth of austenite grain at the temperature of $1250\text{ }^{\circ}\text{C}$. However, when the temperature was more than $1250\text{ }^{\circ}\text{C}$, the pinning effect declined due to the precipitate dissolution. The precipitates and austenite grain coarsening took place with the temperature increasing. Medina et al. (Ref 7) outlined that the precipitates played a strong pinning effect on grain in the steel with the Ti/N ratio close to 2. And the size of precipitates increased with the temperature increasing. He et al. (Ref 8) reported that the growth of austenite grain occurred around $1100\text{ }^{\circ}\text{C}$ in the steel with Zr/N ratios of 2.8 to 6.3. Oxide particles have good ability to pin the austenite grain boundaries at higher temperatures (more than $1400\text{ }^{\circ}\text{C}$), due to the higher melting point. Liu et al. (Ref 9) suggested that the Zr-Al-Ti oxide particles can refine grain in the HSLA steels at the temperature of $1350\text{ }^{\circ}\text{C}$. Li et al. (Ref 10) demonstrated that the fine austenite grain was obtained at the temperature of $1400\text{ }^{\circ}\text{C}$ in the steel containing Mg. That was attributed to the formation of Mg oxide particles. Shi et al. (Ref 11) illustrated that a large amount of fine Zr oxide particles worked to pin the austenite grain boundaries at temperature up to $1400\text{ }^{\circ}\text{C}$ in the steels containing Zr.

Intragranular acicular ferrite (IAF) is considered as the optimum microstructure to improve the mechanical properties of welded joints, especially on the toughness. Lei et al. (Ref 12) revealed that the specimen with Zr content of 0.013% had good impact toughness in the CGHAZ by simulation with 100 kJ/cm heat input due to significant amount of IAF formation in the experimental steel. As reported in our previous studies (Ref 13), excellent impact toughness was obtained in the simulated CGHAZ with heat input in the range 100-1000 kJ/cm. The oxide particles played a significant role in assisting IAF nucleation, improving the mechanical properties in HAZ, especially on low temperature impact toughness. As mentioned above, most researches primarily focused on the microstructure

Pengyan Zhang, School of Metallurgical Engineering, Anhui University of Technology, Maanshan 243032, China; and **Jian Zhang** and **Binzhou Li**, Ansteel Beijing Research Institute, Beijing 102211, China. Contact e-mail: mjzt_2014@126.com.

and impact toughness in HAZ with high-heat input welding by simulation. The research on microstructure transformation and mechanical properties for welded joints with high-heat input welding by actual welding has rarely been studied. However, welding residual stress is one of most main factors on unstable fractures in brittle materials under low temperature service conditions (Ref 14, 15). The relationship of the microstructure and toughness in HAZ between actual welding and simulated welding is of great significance to the evaluation of actual welded joints.

In addition, the electro-gas vertical welding is a typical welding method in shipbuilding (Ref 16). The purpose of this work is to study the microstructure evolution and mechanical properties for welded joints after electro-gas vertical welding under high-heat input condition. We compared the microstructure and impact toughness in HAZ between actual welding and simulated welding. The effect of oxide particles on the nucleation for IAF will be investigated.

2. Materials and Experimental Procedures

The experimental steel (200 kg) was made by a vacuum induction melting furnace (250 kg-150 kW). The ingot was heated to 1200 °C for 2 h and rolled into 30 mm thickness steel plate by thermo-mechanical control processing (TMCP) using a $\Phi 450$ experimental mill, following cooling to 600-610 °C (cooling rate of 20-30 °C/s) by water. Finally, the plate was cooled to room temperature by air cooling. According to ASTM E8, standard round tensile samples with the gage length of 50 mm and diameter of 8 mm were prepared from hot rolled steel plates along the transverse direction. Mechanical properties were measured using a CMT-5105 testing machine at room temperature in a cross-head speed of 3 mm/min. Every tensile test was repeated once. Obviously, the experimental steel as rolled condition meets the requirements of China Classification Society (CCS) and ISO 9000 for the EH40 ship plate steel. The chemical composition and mechanical properties for experimental steel are presented in Table 1. The carbon equivalent and welding crack susceptibility index P_{cm} for experimental steel are 0.354% and 0.166%, respectively, and they were given by Eqs. 1 and 2 (Ref 17)

$$P_{cm} = C + \frac{Si}{30} + \frac{Mn + Cu + Cr}{20} + \frac{Ni}{60} + \frac{Mo}{15} + \frac{V}{10} + 5B \quad (\text{Eq 1})$$

$$CE = C + (Mn/6 + Cr + V + Mo)/5 + (Cu + Ni)/15 \quad (\text{Eq 2})$$

The experimental steel was machined into the plate with dimensions of 500 mm \times 200 mm \times 30 mm for electro-gas vertical welding. The electro-gas vertical welding was conducted using a Lincoln IDEALARC-DC-1000 power and the shape of the groove was a single V with 14 ° based on the Chinese welding standard of GB/T 12470. A flux cored wire (DWS-43G) with 1.6 mm in diameter was selected from Kobe Steel. The chemical composition and mechanical properties for DWS-43G are presented in Table 2. The plates for electro-gas vertical welding are at room temperature without preheating. Main welding parameters were shown in Table 3. Figure 1 presents the photograph of experimental steel plate after electro-gas vertical welding.

In order to investigate the microstructure and toughness at CGHAZ, the thermal simulator was used to simulate the high heat input welding thermal cycle. The specimens for welding simulation were machined into the size of 11 mm \times 11 mm \times 55 mm from the steel plate as rolled. According to the Rykalin mathematical heat transfer model, the high heat input welding thermal cycle of 120, 280,400, and 500 kJ/cm was carried out (Ref 18). The K-type thermocouple was used to monitor the variation of temperature. The heat input energy (E) is the function as the cooling time from 800 °C to 500 °C ($t_{8/5}$). The high-heat input welding thermal cycle main parameters are listed in Table 4.

After electro-gas vertical welding, standard round tensile samples were prepared along the transversal direction of welding pass. According to the CCS “Materials and Welding Code”, the Charpy-V notch location was fixed at different regions of welded joint, as shown in Fig. 2. According to ASTM E23 standard, the samples with 10 mm \times 10 mm \times 55 mm for Charpy-V impact test were prepared. The impact testing was carried out at -20 °C on an Instron Dynatup 9200 impact tester and every test repeated two times due to the narrow width of HAZ (Fig. 3).

The location for metallographic specimen was the same as Charpy-V notch location. These specimens were prepared using standard methods such as grinding, polishing, and then were etched with 4% nital for optical microscope and FEI Quanta 6000 scanning electron microscope (SEM) observation. The chemical distribution of the inclusions assisting the intragranular acicular ferrite nucleation was analyzed by the electron probe micro-analyzer (EPMA-1720).

3. Results

Figure 4 shows the microstructure for the cross section of the whole weld after electro-gas vertical welding, including heat affected zone (HAZ) and welded metal (WM). The microstructure consisted of intragranular acicular ferrite (IAF),

Table 1 Chemical composition and mechanical properties for experimental steel as-rolled

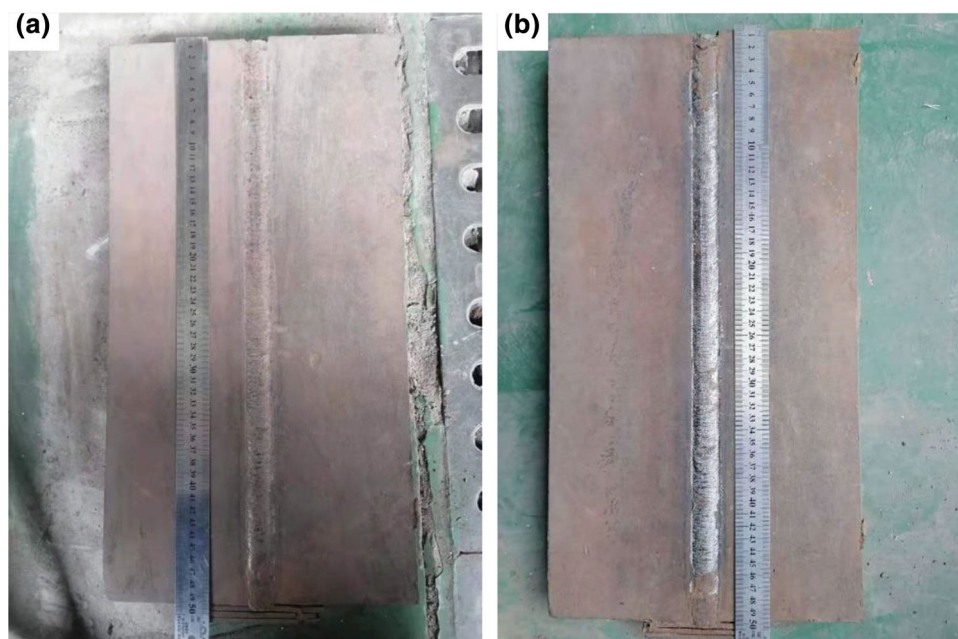
Chemical composition, wt %								Mechanical properties				
C	Si	Mn	P	S	Ti	Cr+Mo+Cu+Ni	Fe	Yield Strength, MPa	Ultimate Tensile Strength, MPa	Yield-to-Tensile Strength Ratio	Elongation, %	$A_{KV}(-20^\circ\text{C}), \text{J}$
0.08	0.20	1.50	0.008	0.003	0.018	<0.1	Bal.	440	560	0.81	29	310

Table 2 Chemical composition and mechanical properties for DWS-43G

C	Si	Mn	Mo	Yield strength, MPa	Ultimate tensile strength, MPa	Elongation, %	A_{KV} , - 20 °C, J
0.08	0.35	1.63	0.17	470	600	27	62

Table 3 Main parameters for electro-gas vertical welding

Plate thickness, mm	Welding current, A	Welding voltage, V	Welding speed, cm/min	Heat input, kJ/cm
30	400	44	5.1	207

**Fig. 1** Photograph for the front side (a) and (b) reverse side of experimental welded plate**Table 4 Main parameters for welding thermal simulation**

Heat input, kJ/cm	Peak temperature, °C	Holding time, s	$t_{8/5}$, s
120	1400	3	198
280	1400	3	269
400	1400	3	325
500	1400	3	550

intragranular ferrite (IGF) and grain boundary ferrite (GBF) near fusion line (FL). The left side of FL is the HAZ, and the right side of FL is the WM. It is found that the microstructure size for WM is finer than that of HAZ. In addition, the amount of IAF for WM is higher than that of HAZ.

Mechanical properties for specimens of welded joint after electro-gas vertical welding are shown in Table 5. The mechanical properties meet the requirements of the CCS “Materials and Welding Code”. An increase in the absorbed energy for the position away from fusion line (FL) is observed. Solid phase transformation occurred in HAZ during welding, leading to microstructure softening. Furthermore, the microstructure for WM has high hardenability due to much

more alloys, as shown in Table 2, resulting in HAZ fracture after tensile test, as shown in Fig. 3.

Figure 5 shows that the microstructure for HAZ by simulation. The microstructure seem to be the same as the electro-gas vertical welding, mainly consisting of IAF, IGF and GBF. It can be seen that the amount of GBF and IGF for HAZ by simulation increased as the heat input increasing. The GBF and IGF belong to the diffusive transformation mechanism. The growth for both microstructures was mainly related to the temperature and time. When the heat input was 500 kJ/cm, GBF and IGF size become coarsen, because higher heat input welding thermal cycle provides the longer cooling time from 800 to 500 °C. There seem to be little variation in austenite

grain size for HAZ by simulation. Because the austenite grain size mainly depends on the austenitization parameters and steel chemical composition.

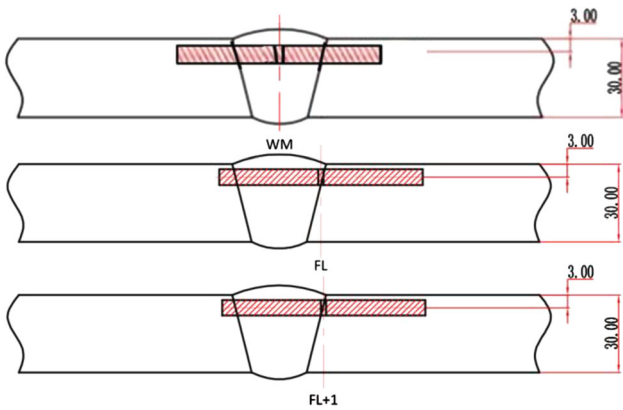


Fig. 2 Schematic of the Charpy-V notch location in electro-gas vertical welding

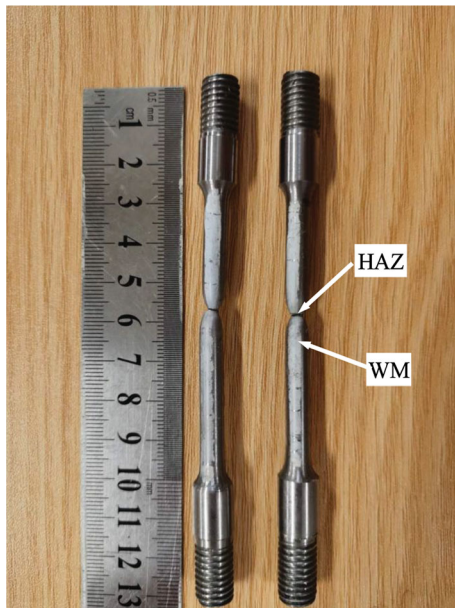


Fig. 3 Tensile specimens for welded joint

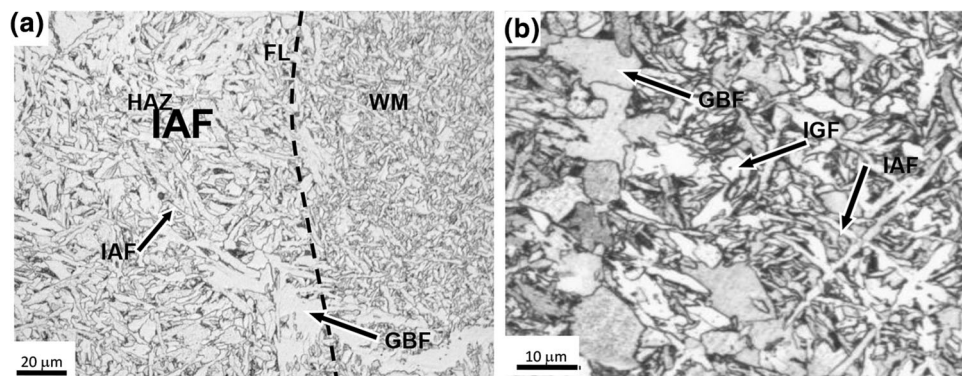


Fig. 4 Typical microstructure of electro-gas vertical welding near fusion line (a) and in HAZ (b)

Figure 6 shows the average absorbed energy for HAZ by simulation at $-20\text{ }^{\circ}\text{C}$. The absorbed energies consistently decreased with heat input increasing. The average absorbed energy of specimens for HAZ with 120, 280, 400 and 500 kJ/cm heat input is 177, 137, 131 and 101 J, respectively. The specimens share the identical process history and chemical composition except the $t_{8/5}$. It is reported by Shi et al. (Ref 19) that the impact energy for HAZ is not only related with the volume fraction of IAF but also with that of GBF. The cracks tend to propagate on the large GBF.

It was found that the average impact energy (177 J) for HAZ by simulation with heat input of 120 kJ/cm is similar with that (165 J) for FL+1 mm by electro-gas vertical welding with heat input of 207 kJ/cm. It can be inferred that the specimen experienced welding thermal cycle by simulation is stricter than that of electro-gas vertical welding. It is difficult to measure the accurate value of impact energy for HAZ in actual welding, because the width of HAZ is so narrow due to temperature gradient caused by welding thermal cycle. The impact energy for HAZ is susceptible to the notch location. In addition, the fusion line is usually arc line rather than straight line; the notch region more or less includes the microstructure of FL and HAZ, because a certain angle groove is good for improving the mechanical properties for welded joints in actual welding. It is convenient and feasible to study the impact toughness for HAZ by use of simulation.

4. Discussions

It is recognized that the HAZ is the weakest region in welded joints, especially on the impact toughness at low temperature. The impact toughness for HAZ can be improved by the following two ways: (1) Inhibiting the excessive coarsening of the prior austenite grain; (2) Refining the microstructure with the help of the IAFs (Ref 20). The high melting point inclusions were typically used to achieve the above two purposes.

4.1 Effect of Titanium Compounds on the Prior Austenite Grain Size

Figure 7 presents the morphology of the titanium compounds at the austenite grain boundary in HAZ by simulation with heat input of 500 kJ/cm. The TiN inclusion is usually a distinct rectangular shape. However, the presentation of the

Table 5 Mechanical properties for welded joint

Ultimate tensile strength, MPa	Cold bending, 180°	Fracture location	Sampling location	A_{kv} , -20°C, J	Average A_{kv} , -20°C, J
530; 535	Eligible	HAZ	WM	86,72,91	83
			FL	102,128,139	123
			FL+1mm	175,155,166	165

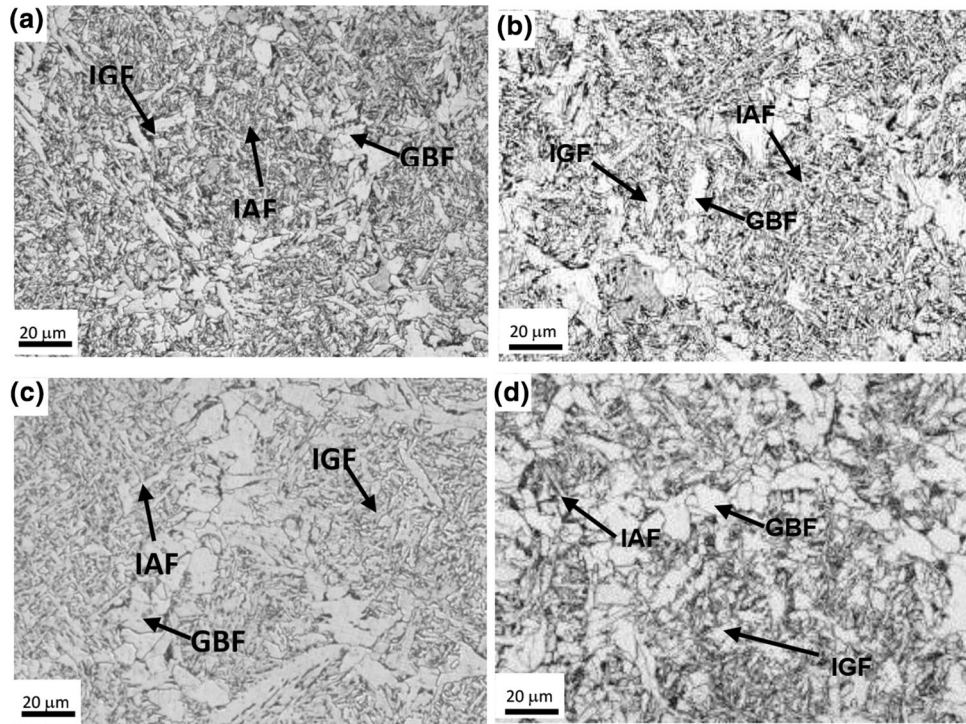


Fig. 5 Typical microstructure of HAZ with heat input of 120 kJ/cm (a), 280 kJ/cm (b), 400 kJ/cm (c) and 500 kJ/cm (d)

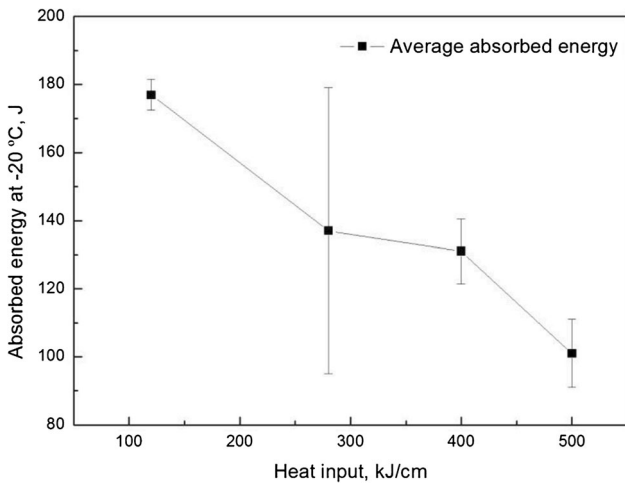


Fig. 6 Charpy impact energies for HAZ by simulation

ellipse TiN indicated that the TiN inclusion was partially dissolved in GBF, as shown in Fig. 6(a).

In the traditional high-heat input welding steel, the inhibition of the austenite grain coarsening was achieved through the “pinning effect” of the TiN particles (Ref 21). As the temperature increasing, the volume fraction of TiN decreases.

It is suggested by Koda et al. (Ref 22) that the TiN inclusions begin to partially dissolve—the dissolved volume fraction was about 50% when the temperature reached 1350 °C. Most of the TiN inclusions were dissolved—the dissolved volume fraction was about 88% when the temperature was around 1400 °C. In the present study, the peak temperature is 1400 °C, the TiN loss the pinning effect in HAZ. However, the titanium oxide particles play a significant role in inhibiting the austenite grain growth because of the high melting point. The titanium oxide inclusion was observed near the GBF and two IAFs nucleated on the composite inclusion (TiO_x -MnS) toward the grain, as shown in Fig. 6(b). The observation is consistent with the conclusion by Shi et al. (Ref 11). They have reported that the oxide inclusion acted as pinning particles at the austenite grain boundaries on heating to 1400°C for 100s.

During cooling, the GBFs firstly nucleated at the austenite grain boundaries due to the lower activation energies, and then the IAFs heterogeneously nucleated on the composite inclusions. If the titanium oxide distributed at the austenite grain boundaries, they can prevent the growth of austenite grain and assist the formation of IAFs.

4.2 Effect of Titanium Compounds on IAF

It is usually believed that the IGF with an aspect ratio higher than 3:1 is termed as IAF (Ref 23). The IAF is a typical

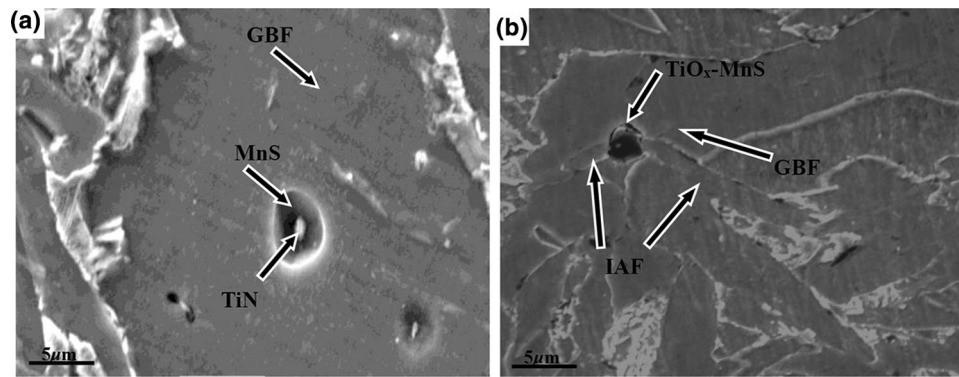


Fig. 7 Titanium compound near GBFs in HAZ by simulation with heat input of 500 kJ/cm

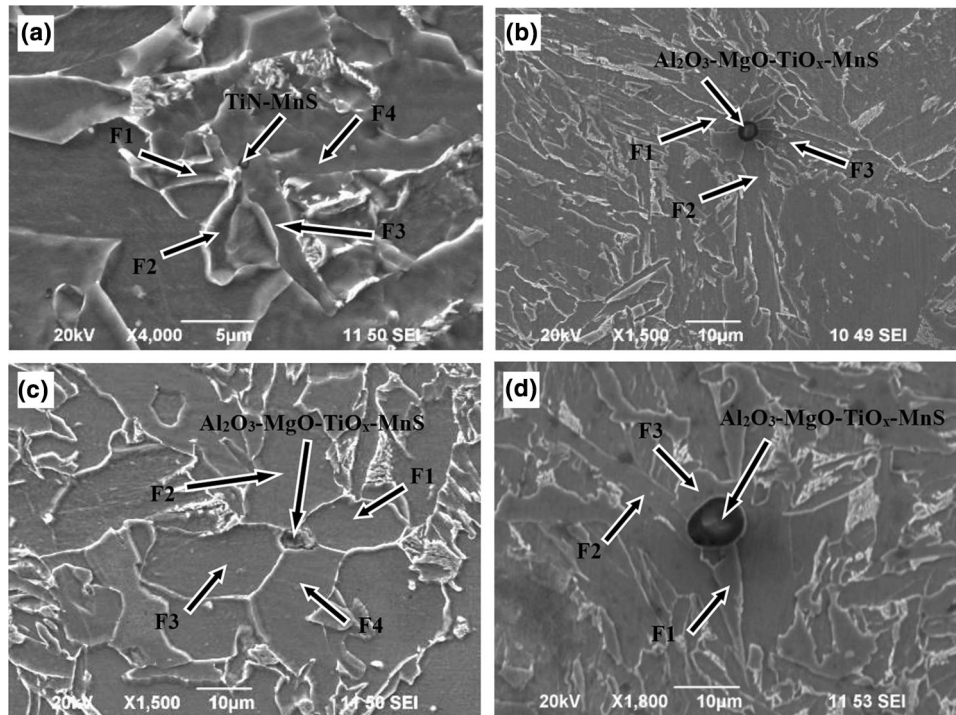


Fig. 8 Nucleation of IGFs and IAFs on the typical inclusions in the HAZ by electro-gas vertical welding

microstructure in HAZ and WM, providing the optimum HAZ and WM mechanical properties with respect to strength and toughness. Because the IAF is characterized by a cross-shaped morphology and functions as high-angle grain boundaries to efficiently improve the impact toughness.

The formation of IAF is related to the inclusion size except the chemical composition and welding thermal cycle. During the austenite to ferrite transformation, the new phase sites of heterogeneous nucleation were provided by the phase interface. The formation of the GBF was determined by the total grain boundary area due to the nucleation in the grain boundary. Similarly, the formation of the IAF was determined by the inclusion size as a result of the nucleation of the IAF on the inclusion surface. When the inclusion size was too small, the phase interface also decreased. Thus, the requirement of the critical interfacial area of the heterogeneous nucleation was not

satisfied, hindering the growth of the IAFs on the inclusion. While the inclusion was too large, the phase interface functioned as the grain boundary, and the formation of the massive ferrites was promoted. Therefore, the nucleation of the IAFs was promoted in a range of inclusion sizes. It is found by Ricks et al. (Ref 24) and Barbaro et al. (Ref 25) that the particle minimum size for the most favorable IAF nucleation was about 400 nm. Figure 7(a) shows that the IAFs nucleated on a TiN-MnS particle with the size of 620 nm in the HAZ by electro-gas vertical welding. It is obvious that four IAFs presented in the HAZ with the help of the particle. It is reported by Hong et al. (Ref 26) and Pan et al. (Ref 27) that the oxide particle with MnS minimum size for the most favorable IAF nucleation was less than 3 µm. Figure 7(b) shows that the IAFs nucleated on a TiO_x-Al₂O₃-MgO-MnS particle with the size of 2.5 µm in the HAZ by electro-gas vertical welding. The formation of three

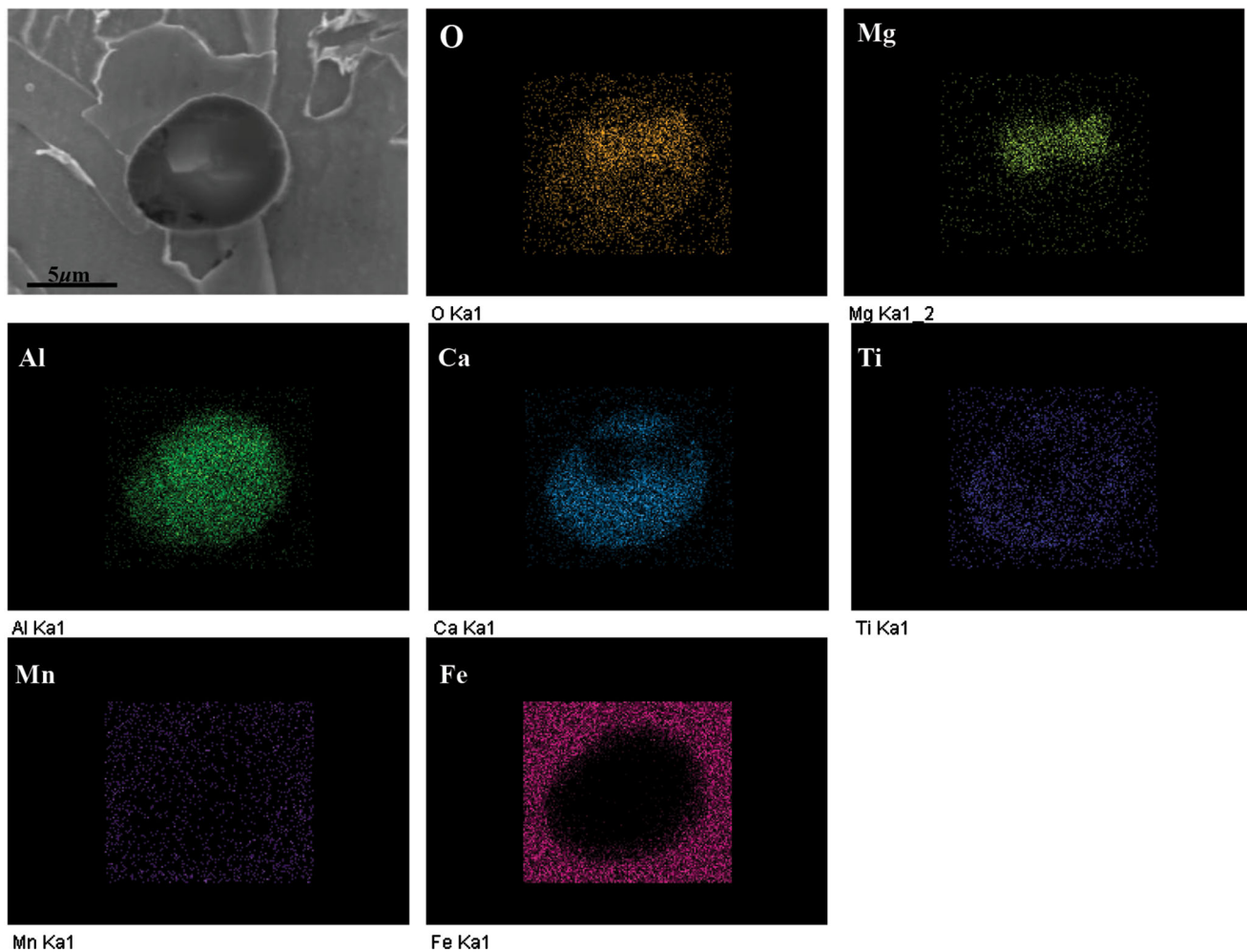


Fig. 9 Map scanning for the inclusion assisting the IAFs nucleation

IAFs nucleated on the composite inclusion was observed. Takamura et al. (Ref 28) has proposed that the size of the inclusion is larger than $5\mu\text{m}$, the IGF growth is not promoted by the inclusions, and microcracks were formed, reducing the toughness for the HAZ. However, the nucleation of IGFs and IAFs on the larger particle (more than $5\mu\text{m}$) was still observed in the HAZ by electro-gas vertical welding. Four IGFs (aspect ratio less than 3:1) nucleated on the $\text{TiO}_x\text{-Al}_2\text{O}_3\text{-MgO-MnS}$ particle with the size of $6.4\mu\text{m}$, as shown in Fig. 8(c). Three IAFs nucleated on the $\text{TiO}_x\text{-Al}_2\text{O}_3\text{-MgO-MnS}$ particle with the size of $7.6\mu\text{m}$, as shown in Fig. 8(d). In the present work, the inclusion size is not the dominant factor on the nucleation of IGFs and IAFs.

To analyze the chemical composition of the inclusion assisting the IAFs nucleation, map scanning and line scanning for the inclusion with the size of $7.6\mu\text{m}$ assisting the IAFs nucleation in HAZ by the electro-gas vertical welding were conducted by EPMA, as shown in Fig. 9 and 10. It was found that the distribution of the Al, Mn, O and Ti in the IAF grain was uniform and stable, basically maintaining a small and constant variation. However, the concentrations of these elements gradually increased in the inclusion until it reached a peak from the starting point. Previous studies (Ref 29-31) have shown that TiO could be nucleated on the surface of the

inclusions in the Ti-containing steel, which is favorable for the nucleation of MnAl_2O_4 due to the addition of Mn and Al into experimental steels, as well as the nucleation of IAFs. Table 6 lists the lattice matching between the particles and ferrite (Ref 32). It is indicated that MnAl_2O_4 and TiO particle have good lattice matching with ferrite, 1.8% and 3.0%, respectively. They have a strong ability to promote the nucleation of IAF. However, the value for MnS is 8.8%, which is not favorable for the nucleation of IAFs.

5. Conclusions

- (1) The experimental steel (EH40 ship plate steel) exhibited excellent impact toughness at -20°C after electro-gas vertical welding with heat input of 207 kJ/cm . The average impact energy at -20°C for WM, FL and FL+1mm is 83 J, 123 J and 165 J, respectively. The average impact energy at -20°C for the HAZ by simulation with heat input of 120 kJ/cm , 280 kJ/cm , 400 kJ/cm and 500 kJ/cm is 177 J, 137J, 131 J and 101 J, respectively. The

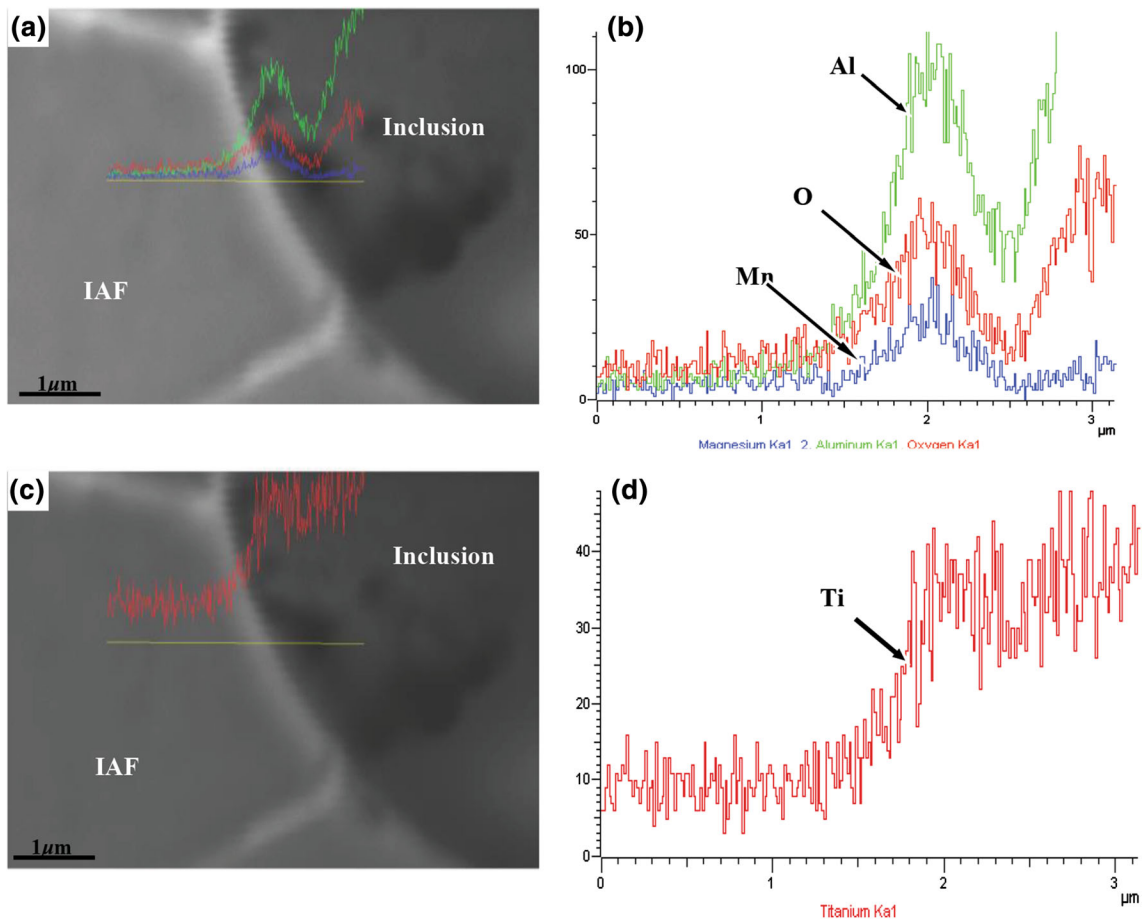


Fig. 10 Line scanning for the inclusion assisting the IAFs nucleation

Table 6 Misfit values between different substrates and ferrite (Ref 29)

Substrate	Relation of planes between nucleating substrate (S) and α Fe	Misfit, %
MnAl ₂ O ₄	{100}S//{100} α Fe	1.8
TiO	{100}S//{100} α Fe	3.0
TiN	{100}S//{100} α Fe	4.6
BN	{110}S//{100} α Fe	6.5
CuS	{111}S//{111} α Fe	2.8
MnS	{111}S//{111} α Fe	8.8
Al ₂ O ₃	{0001}S//{111} α Fe	16.1

specimen experienced welding thermal cycle by simulation is stricter than that of electro-gas vertical welding. It is convenient and feasible to study the impact toughness for HAZ by use of simulation.

- (2) The GBF and IGF size increased in the HAZ with the heat input increasing. The TiN particle lost the pinning effect when the peak temperature reached 1400 °C. However, the titanium oxide particles play an important role in inhibiting the austenite grain growth because of the high melting point.
- (3) In the present study, three IAFs nucleated on the TiO_x-Al₂O₃-MgO-MnS particle with the size of 7.6 μ m were observed. The inclusion size is not the dominant

requirement for the nucleation of IGFs and IAFs. The MnAl₂O₄ and TiO particle have good lattice matching with ferrite, they have a strong ability to promote the nucleation of IAF. However, the lattice matching for MnS with ferrite is 8.8%, which is not favorable for the nucleation of IAFs.

Acknowledgment

This work was supported by a grant from National Natural Science Foundation Project of China (Grant Number 51674004)

Conflicts of interest

The authors declare no conflict of interest.

References

1. M.H. Shi, X.G. Yuan, H.J. Huang, and S. Zhang, Effect of Zr Addition on the Microstructure and Toughness of Coarse-Grained Heat-Affected Zone with High-Heat Input Welding Thermal Cycle in Low-Carbon Steel, *J. Mater. Eng. Perf.*, 2017, **26**(7), p 1–9. <https://doi.org/10.1007/s11665-017-2758-8>
2. W.Z. Mu, P.G. Jonsson, and K. Nakajima, Recent Aspects on the Effect of Inclusion Characteristics on the Intragranular Ferrite Formation in Low Alloy Steels: A Review, *High Temp. Mater. Proc.*, 2017, **36**(4), p 309–325. <https://doi.org/10.1515/htmp-2016-0175>
3. J. Kobayashi, D. Ina, A. Futamura, and K. Sugimoto, Fracture Toughness of an Advanced Ultrahigh-strength TRIP-aided Steel, *ISIJ Int.*, 2014, **54**(4), p 955–962. <https://doi.org/10.2355/isijinternational.54.955>
4. K. Seo, H. Ryoo, and H.J. Kim, Local Variation of Impact Toughness in Tandem Electro-Gas Welded Joint, *Weld. World*, 2020, **64**(3), p 457–465. <https://doi.org/10.1007/s40194-019-00844-8>
5. M.H. Lee, R. Kim, and J.H. Park, Effect of Nitrogen on Grain Growth and Formability of Ti-Stabilized Ferritic Stainless Steels, *Sci. Rep.*, 2019, **9**(1), p 1–11. <https://doi.org/10.1038/s41598-019-42879-3>
6. Q.Y. Sha and Z.Q. Sun, Grain Growth Behavior of Coarse-Grained Austenite in a Nb-V-Ti Microalloyed Steel, *Mater. Sci. Eng. A.*, 2009, **523**, p 77–84. <https://doi.org/10.1016/j.msea.2009.05.037>
7. S.F. Medina, M. Chapa, P. Valles, A. Quispe, and M.I. Vega, Influence of Ti and N Contents on Austenite Grain Control and Precipitate Size in Structural Steels, *ISIJ Int.*, 1999, **39**(9), p 930–936. <https://doi.org/10.2355/isijinternational.39.930>
8. K. He and T.N. Baker, Effect of Zirconium Additions on Austenite Grain Coarsening of C-Mn and Microalloy Steels, *Mater. Sci. Eng. A.*, 1998, **256**, p 111–119. [https://doi.org/10.1016/S0921-5093\(98\)00804-1](https://doi.org/10.1016/S0921-5093(98)00804-1)
9. Y. Liu, G.Q. Li, X.L. Wan, X.G. Zhang, Y. Shen and K.M. Wu, Toughness Improvement by Zr Addition in the Simulated Coarse-Grained Heat-Affected Zone of High-Strength Low-Alloy Steels, *Ironmak. Steelmak.*, 2019, **46**, p 113–123. <https://doi.org/10.1080/03019233.2017.1353763>
10. X.B. Li, T.S. Zhang, Y. Min, C.J. Liu and M.F. Jiang, Effect of Magnesium Addition in Low-Carbon Steel Part 1: Behaviour of Austenite Grain Growth, *Ironmak. Steelmak.*, 2019, **46**, p 292–300. <https://doi.org/10.1080/03019233.2017.1368953>
11. M.H. Shi, K. Rangasayee, J. Zhang, X.G. Yuan, L.J. Li, Effect of Zr Microalloying on Austenite Grain Size of Low-Carbon Steels, *Metal. Mater. Trans. B.*, 2019, **50**(6), p 2574–2585. <https://doi.org/10.1007/s11663-019-01701-1>
12. J.W. Lei, K.M. Wu, Y. Li, T.P. Hou, X. Xie, and R.D.K. Misra, Effects of Zr Addition on Microstructure and Toughness of Simulated CGHAZ in High-Strength Low-Alloy Steels, *J. Iron Steel Res. Int.*, 2019, **26**(10), p 1117–1125. <https://doi.org/10.1007/s42243-019-00319-6>
13. M.H. Shi, P.Y. Zhang, C. Wang, and F.X. Zhu, Effect of High Heat Input on Toughness and Microstructure of Coarse Grain Heat Affected Zone in Zr Bearing Low Carbon Steel, *ISIJ Int.*, 2014, **54**(4), p 932–937. <https://doi.org/10.2355/isijinternational.54.932>
14. G. An, J. Park, and I. Han, Effects of High Toughness and Welding Residual Stress for Unstable Fracture Prevention, *Appl. Sci.*, 2020, **10**(23), p 1–14. <https://doi.org/10.3390/app10238613>
15. V. Richter-Trummer, P.M.G.P. Moreira, J. Ribeiro, and P.M.S.T. Castro, The Contour Method for Residual Stress Determination Applied to an Friction Stir Butt Weld, *Mater. Sci. Forum*, 2011, **681**, p 177–181. <https://doi.org/10.4028/www.scientific.net/MSF.681.177>
16. K. Seo, H. Ryoo, and H.J. Kim, Characterization of the local Brittle Layer Formed in Electro-Gas Weld Metals, *Weld. World*, 2021, **65**, p 513–524. <https://doi.org/10.1007/s40194-020-01032-9>
17. B.D. Meester, The weldability of modern structural TMCP steels, *ISIJ Int.*, 1997, **37**(6), p 537–551. <https://doi.org/10.2355/isijinternational.37.537>
18. N. Rykalin, *Calculation of Heat Processes in Welding*, 1st ed. Mashgiz, Moscow, 1960, p 4–6
19. M.H. Shi, P.Y. Zhang, and F.X. Zhu, Toughness and Microstructure of Coarse Grain Heat Affected Zone with High Heat Input Welding in Zr-bearing Low Carbon Steel, *ISIJ Int.*, 2014, **54**(1), p 188–192. <https://doi.org/10.2355/isijinternational.54.188>
20. Y. Tanimoto, H. Terasaki, and Y.I. Komizo, In-situ Observation of Microstructure Evolution in Heat-Affected-Zone of Ti-Killed Steel Weld, *Q. J. Jpn. Weld. Soc.*, 2009, **27**, p 122–125. <https://doi.org/10.2207/qjws.27.122s>
21. N. Fujiyama, T. Nishibata, H. Hirata, and A. Seki, Analysis of γ Grain Growth Behavior with TiN Dissolution, *Prep. Nat. Meet. JWS*, 2013, **21**, p 176–177
22. M. Koda, K. Amano, Y. Funahashi, C. Shiga, and S. Ueda, Relation Between Solution Behavior of TiN Particles and Austenite Grain Size in Synthetic HAZ (Properties of Iron and Steel), *Tetsu. Hagane.*, 1984, **70**, p S1265
23. T. Koseki and G. Thewlis, Overview Inclusion Assisted Microstructure Control in C-Mn and Low Alloy Steel Welds, *Mater. Sci. Tech.*, 2005, **21**(8), p 867–879. <https://doi.org/10.1179/174328405x51703>
24. R.A. Ricks, P.R. Howell, and G.S. Barritte, The Nature of Acicular Ferrite in HSLA Steel Weld Metals, *J. Mater. Sci.*, 1982, **17**, p 732–740. <https://doi.org/10.1007/BF00540369>
25. F.J. Barbaro, P. Krauklis, and K.E. Eastering, Formation of Acicular Ferrite at Oxide Particles in Steels, *Mater. Sci. Tech.*, 1989, **5**, p 1057–1068. <https://doi.org/10.1179/026708389790340888>
26. S.G. Hong, K.J. Kang, and C.G. Park, Strain-Induced Precipitation of NbC in Nb and Nb-Ti Microalloyed HSLA Steels, *Scr. Mater.*, 2002, **6**, p 163–168. [https://doi.org/10.1016/S1359-6462\(01\)01214-3](https://doi.org/10.1016/S1359-6462(01)01214-3)
27. Y.T. Pan and J.L. Lee, Development of TiOx-bearing steels with superior heat-affected zone toughness, *Mater. Des.*, 1994, **15**, p 331–338. [https://doi.org/10.1016/0261-3069\(94\)90027-2](https://doi.org/10.1016/0261-3069(94)90027-2)
28. J. Takamura, S. Mizoguchi, Roles of Oxides in Steel Performance, in proceedings of the 6th internal iron and steel congress. (Nagoya, ISIJ, 1999), pp. 591–597
29. Hori. Effect of Chemical Composition on Strength and Toughness of Welds Made by Large Heat Input Submerged Arc Welding. PhD Thesis, Osaka University, 1995
30. S. Tsumishima, S. Ohkita, and Y. Hori, Effects of Oxygen on the Toughness of Ti-B Containing AC-MIG Weld Metal Development of AC-MIG Welding Process (Report 3), *Q. J. Jpn. Weld. Soc.*, 1992, **10**, p 264–271. <https://doi.org/10.2207/qjws.10.264>
31. J.M. Dowling, J.M. Corbett, and H.W. Kerr, Inclusion Phases and the Nucleation of Acicular Ferrite in Submerged arc Welds in HIGH Strength Low Alloy Steels, *Metal. Mater. Trans. A.*, 1986, **17A**, p 1611–1623. <https://doi.org/10.1007/BF02650098>
32. Y. Tomonori, Study on inclusion composition and acicular ferrite formation behavior in weld metal of Ti-B low carbon alloy steel. PhD Thesis, Osaka University, 88–89, 2009

Publisher's Note Springer Nature remains neutral with regard to jurisdictional claims in published maps and institutional affiliations.